energies

MDPI

Article

Electrochemical Performance of a Hybrid $NiCo_2O_4$@NiFelt Electrode at Different Operating Temperatures and Electrolyte pH

Ataollah Niyati, Arianna Moranda *, Pouya Beigzadeh Arough, Federico Maria Navarra and Ombretta Paladino *

Department of Civil, Chemical and Environmental Engineering, University of Genoa (UNIGE-DICCA), Via All'Opera Pia 15, 16145 Genoa, Italy; ataollah.niyati@edu.unige.it (A.N.)

* Correspondence: arianna.moranda@edu.unige.it (A.M.); paladino@unige.it (O.P.)

Abstract: Transition metals such as nickel and cobalt as an alternative to Pt and Pd can be used for oxygen evolution reactions (OERs) and hydrogen production reactions (HERs) in alkaline environments, facilitating green hydrogen production as a sustainable alternative to fossil fuels. In this study, an $NiCo_2O_4$ catalyst was produced by a sono-hydrothermal method using urea as a hydrolysis agent. The electrochemical performance of the catalyst-coated NiFelt electrode was evaluated at different KOH concentrations (0.25, 0.5, and 1 M) and four operating temperatures in the interval of 20–80 °C. The electrode characteristics were investigated via electrochemical spectroscopy (cyclic voltammetry, EIS, multistep chronopotentiometry, multistep chronoamperometry) using two different reference electrodes (Ag/AgCl and Hg/HgO), to obtain insight into the anodic and cathodic peaks. XRD, SEM, EDS, and TEM analyses confirmed the purity, structure, and nanoscale particle size (20–45 nm) of the $NiCo_2O_4$ catalyst. The electrode showed symmetric CV with Ag/AgCl, making this reference electrode more appropriate for capacitance measurements, while Hg/HgO proved advantageous for EIS in alkaline solutions due to reduced noise. The overpotential of the catalyst-coated NiFelt decreased by 108 mV at 10 mA/cm^2 compared to bare NiFelt, showing a good potential for its application in anion exchange membranes and alkaline electrolyzers at an industrial scale.

Keywords: alkaline electrolyzers; AEM electrolyzers; transition metals; electrocatalyst; Ni–Co metal oxide; sono-hydrothermal; OER; HER

Citation: Niyati, A.; Moranda, A.; Beigzadeh Arough, P.; Navarra, F.M.; Paladino, O. Electrochemical Performance of a Hybrid $NiCo_2O_4$@NiFelt Electrode at Different Operating Temperatures and Electrolyte pH. *Energies* **2024**, *17*, 3703. https://doi.org/10.3390/en17153703

Academic Editor: Antonino S. Aricò

Received: 27 June 2024
Revised: 17 July 2024
Accepted: 24 July 2024
Published: 26 July 2024

1. Introduction

New frontiers in carbon neutrality are driving the world in the direction of green energy through constructing a new system based on environmental sustainability. This direction and the decrease in fossil fuels are opening the way to sustainable energy carriers. Hydrogen is a zero CO_2 emission energy carrier [1,2] since the product of its oxidation is only water.

Currently, the most widespread and developed technologies for the production of hydrogen are those based on traditional methods of using fossil fuels: natural gas reforming and coal gasification. These technologies inevitably cause abundant CO_2 emissions into the atmosphere [3,4].

An alternative and promising way for the production of hydrogen is water electrolysis. This technology, in addition to being CO_2 neutral, acquires further interest if coupled with the use of electricity from renewable energy sources such as solar, wind, etc. [5–8].

Alkaline water electrolyzers (AWE) and anion exchange membrane water electrolyzers (AEMWE) [9] present important peculiarities, thanks to the great interest they have attracted at the industrial scale: transition metals can be used for both oxygen evolution reactions (OERs) and hydrogen evolution reactions (HERs) [10,11]. Since no noble metals are used, electrocatalysts are less expensive and more easily supplied. Although AEMWE

is an emerging technology if compared to AWE, the results obtained at the lab scale and pilot scale show it to be a promising technology, exhibiting performances between alkaline and PEM water electrolysis [12].

Improving the performances of electrocatalysts for both OERs and HERs is of great importance to reduce energy losses and to increase the overall efficiency of the system [13,14]. In particular, finding a performant electrocatalyst for oxygen evolution reactions is a key point to reduce losses due to the four-electron transfer in the redox pair [15]. Numerous studies reported on transition metal oxides for OER improvement in alkaline environments [16–18]. Spinel electrocatalysts are of great interest for their structure, AB_2O_4, where A and B stand for metal ions and characteristics [19–21]. Nickel–cobalt oxides are one of the most interesting catalysts because of their high capacity, excellent redox activity, affordability, and abundant availability in nature [22,23]. Even if the chemical structure is important, the morphology and particle size play a key role in the choice of the electrocatalyst. The engineering of an electrocatalyst must take into account the appropriate shape and size to reduce losses due to mass transport through the porous media of the substrate and improve electrocatalytic activity [24].

$NiCo_2O_4$ has been synthesized in a wide variety of structural forms, spanning nanoparticles [25], nanowires [26], nanoflowers [27], nanosheet arrays [28], and nanoneedle arrays [29], and the results of these studies demonstrate the important role of shape in electrochemical characteristics [30]. Different techniques are used to synthesize spinel Ni–Co metal hydroxide such as decomposition [31], nano casting [32], electrodeposition [33,34], coprecipitation [35], and hydrothermal synthesis [36].

In this study, a sono-hydrothermal method was used to synthesize a $NiCo_2O_4$ electrocatalyst with urea as a hydrolysis agent. Different techniques such as XRD, SEM, EDS, and TEM were adopted to assess the catalyst's physicochemical characteristics. The obtained $NiCo_2O_4$ was then used to produce a hybrid Ni–Co metal oxide@NiFelt electrode, whose electrochemical performances were analyzed at different operating conditions. Moreover, stability tests were carried out at different temperatures and pH, and the after-use structure and composition of the electrode were verified using XRD, SEM, and EDS.

The study also focuses on how the choice of the reference electrode inside the three-electrode setup can influence the results of the electrochemical tests, leading to suggestions on the best choice in terms of parameters to be evaluated.

Based on our study, the use of an Ag/AgCl reference electrode can be convenient with respect to Hg/HgO when the outcome is to achieve capacitance measurements and redox peak detection in cyclic voltammetry. Tests conducted in 0.5 M KOH and 1.0 M KOH using this reference electrode yielded similar results, suggesting the possible use of the lower-cost Ag/AgCl reference electrode at a lower concentration of KOH for lab-scale testing of OER electrocatalysts.

In summary, the main points of this study are the following:

1. Synthesize the $NiCo_2O_4$@NiFelt hybrid electrode using a sono-hydrothermal method followed by annealing, ensuring a binder-free configuration.
2. Evaluate the electrochemical performance of the $NiCo_2O_4$@NiFelt hybrid electrode in terms of overpotential, current density, and stability during the OER process in alkaline media.
3. Examine the influence of operational conditions, including temperature and pH, as well as the choice of reference electrode on the OER performance of the produced electrode.
4. Study the effect of different reference electrodes (Ag/AgCl and Hg/HgO) on electrochemical measurements and provide insights on their suitability for capacitance measurements and/or EIS in alkaline solutions.

2. Materials and Methods

2.1. Chemicals and Materials

Precursors salts $NiCl_2 \cdot 6H_2O$ (99% purity) and $CoCl_2 \cdot 6H_2O$ (98% purity) used for the electrocatalyst synthesis were purchased from Carlo Erba Reagents (Milano, Italy), as well as KOH (99% purity) and urea (99% purity). Ultra-pure deionized water, utilized for all cleaning and synthesis procedures, was procured from Exaxol (Genova, Italy). Ethanol and acetone, employed post-filtration to eliminate any remaining residues, were obtained from Sigma Aldrich (Steinheim, Germany). It should be noted that all the reactants were used as received without further purification.

2.2. Preparation of Hybrid $NiCo_2O_4$@NiFelt Electrode

For synthesizing the hybrid electrode, we chose NiFelt as support material.

In alkaline and anion exchange membrane (AEM) water electrolysis, the use of Ni felt or foam is necessary due to either material's excellent conductivity and catalytic properties.

Ni felt could be better, at an industrial scale, than Ni foam for two main reasons. The cost of production of Ni felt is lower than that of Ni foam; second reason is related to mechanical properties: Ni felt has superior mechanical strength compared to Ni foam, providing better durability and stability during operation at industrial scale.

The synthesis of the $NiCo_2O_4$ on NiFelt is carried out using a sono-hydrothermal process, taking advantage of urea as a hydrolysis agent as described in our previous paper [10]. The sono-hydrothermal synthesis involved several key steps. Figure 1 provides details of the synthesis procedure, starting from synthesizing the electrocatalyst up to carrying out physicochemical analysis and electrochemistry tests.

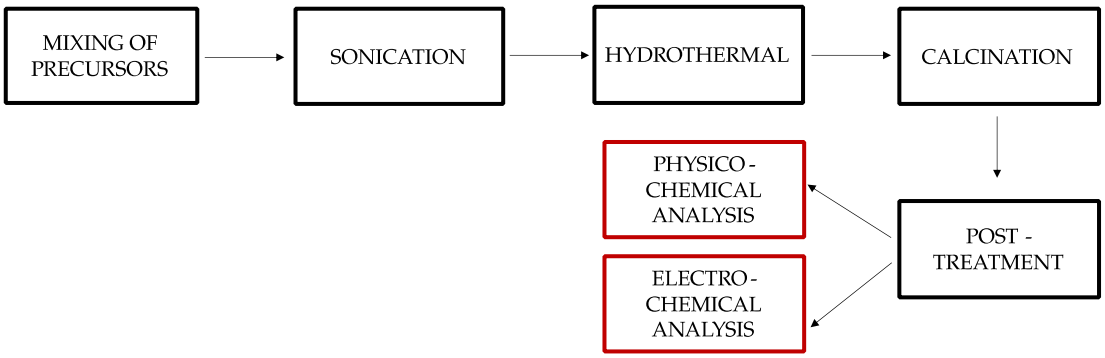

Figure 1. Synthesis procedure with sono-hydrothermal process method and characterizations procedure

First, 2.015 g of $NiCl_2 \cdot 6H_2O$ was dissolved in 25 mL of deionized water (DI) and slowly introduced dropwise into a solution of $CoCl_2 \cdot 6H_2O$, which contained 4.0354 g of the cobalt precursor in 40 mL of DI. Next, urea was added at a molar ratio of 1:10, and the mixture was vigorously stirred for 30 min. The solution was then sonicated for an additional 30 min at 100 W to enhance nucleation and nanoparticle formation. This mixture was transferred to a 100 mL Teflon-lined stainless steel autoclave with an acid-washed NiFelt substrate at the bottom of the autoclave and subjected to a hydrothermal reaction for 10 h at 120 °C. Afterward, the resulting product was washed with DI water and ethanol, filtered, and dried in a vacuum oven at 60 °C. In the final step, the dried product was heated in a furnace at 350 °C for 3 h, with a heating rate of 10 °C/min. The final result is an electrode in which the electrocatalyst is chemically bound to the nickel felt within the entire substrate volume and not only on the surface. As an indication, the final load of the catalyst on the electrode is 7 mg/cm^2.

The mass loading is a key point, since it is strongly related to the oxygen evolution reaction (OER) efficiency. Generally, by increasing the active mass, the catalytic activity is also enhanced due to the higher number of active sites. However, exceeding the optimal amount of catalyst can lead to a decrease in performance due to mass transport limitations and potential blockage of active sites.

2.3. Physicochemical Characterizations

The physical and chemical structures of the $NiCo_2O_4$ powder were examined using a variety of analytical techniques. X-ray diffraction (XRD) was used at room temperature in air with PANalytical AERIS equipment to investigate the crystal structure and phase composition. The sample morphology was evaluated using a TESCAN (Brno, Czech Republic) scanning electron microscope (SEM). Energy-dispersive spectroscopy (EDS), using a Hitachi (Tokyo, Japan) SU3500 detector, allowed us to analyze the $NiCo_2O_4$ powder composition and detect any contaminants in the produced electrocatalyst. Transmission electron microscopy (TEM) was used to analyze the samples' structural composition and morphology using a JEM 2100 Plus apparatus from JEOL Ltd. (Tokyo, Japan).

2.4. Electrochemical Characterization Method

Electrocatalyst measurements were performed using an IVIUM Vertex.10A potentiostat workstation (Ivium Technologies B.V., Eindhoven, The Netherlands) in 0.25, 0.5, and 1.0 M KOH electrolyte solutions. The hybrid $NiCo_2O_4$@NiFelt electrode was used as the working electrode, with Hg/HgO or Ag/AgCl as the reference electrode, and a platinum wire served as the counter electrode. Polarization curves were measured at a scan rate of 5 $mV \cdot s^{-1}$. Cyclic voltammograms (CVs) were recorded at varying scan rates within a specific potential range concerning the specific reference electrode. Electrochemical impedance spectroscopy (EIS) was conducted over a frequency range of 0.01 to 100,000 Hz with 10mV amplitudes. The potential response over time was observed by 1000 CV under a scan rate of 50 mV/s (24 h duration test). Potentials were calibrated to a reversible hydrogen electrode (RHE) in 1.0 M KOH and corrected for the 100% iR drop using the formula $E(RHE) = E_0(Hg/HgO) + 0.105 + 0.059 \times pH - iRs$, $E(RHE) = E_0(Ag/AgCl) + 0.197 + 0.059 \times pH - iRs$, where Rs is the equivalent series resistance obtained from fitting calculations. For the temperature effect, the potential is not corrected concerning the iR drop.

2.5. Electrochemical Performance of Hybrid $NiCo_2O_4$@NiFelt Electrode

The electrochemical performance of the synthesized electrocatalyst on NiFelt was evaluated in a three-electrode setup. A first run of tests was carried out at fixed pH and temperature using two different reference electrodes (REs). This activity allowed us to understand how the use of different REs can highlight different characteristics of the electrocatalyst. Then, tests at different operating temperatures and pH were performed with the chosen RE.

3. Results and Discussion

3.1. Physicochemical Characterizations of $NiCo_2O_4$ Catalyst Powder

As a starting point for analyzing the physicochemical properties of $NiCo_2O_4$ electrocatalyst powder, XRD, SEM, EDS, and TEM analyses were performed; the results are shown in Figure 2.

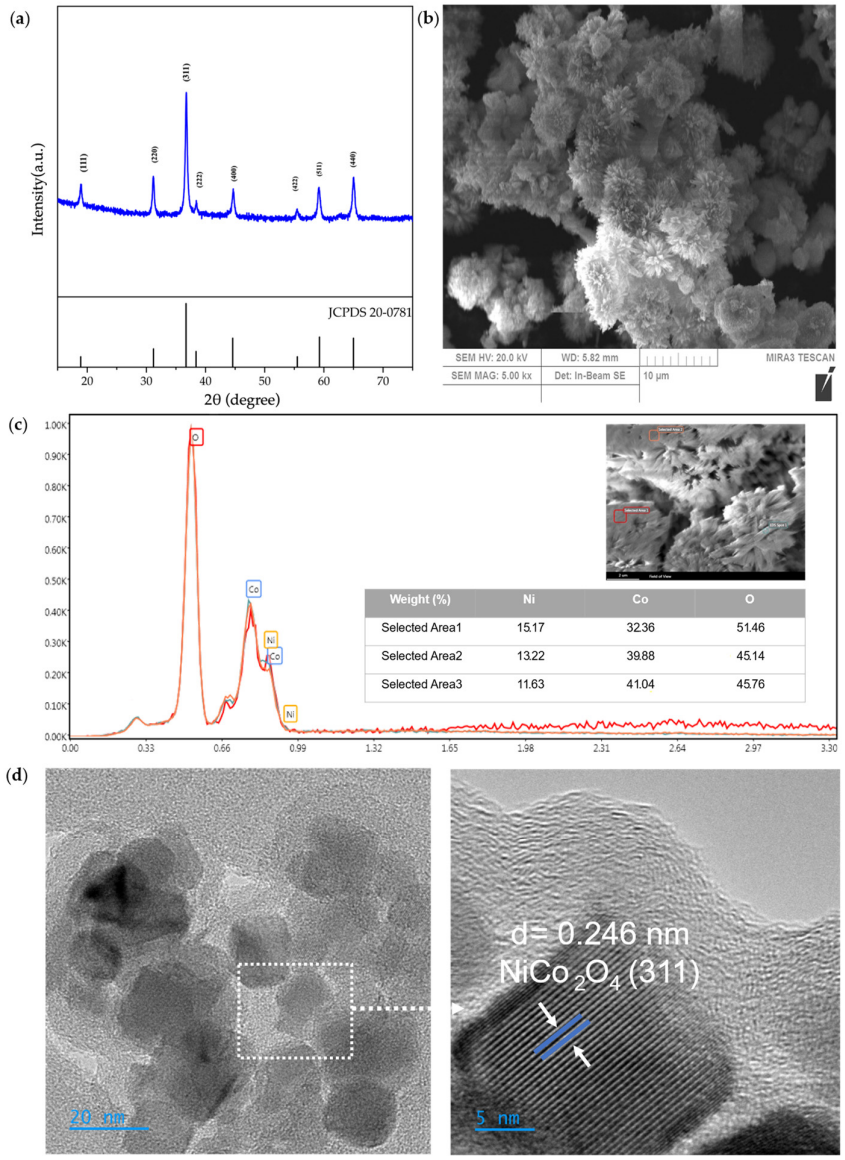

Figure 2. Physicochemical characterization of Ni–Co metal oxide: (**a**) XRD, (**b**) SEM (SEM MAG: 5.00 kx), (**c**) EDS, (**d**) TEM.

XRD analysis is reported in Figure 2a; it can provide insights into the crystal structure and composition of Ni–Co metal oxide, and it was carried out for 2θ = 20–80°. Peaks were found at 18.90°, 31.15°, 36.70°, 38.40°, 44.62°, 55.43°, 59.09°, 64.98°, and 77.54°, which correspond to the crystallographic planes (111), (220), (311), (222), (400), (422), (511), (440), and (533) of cubic $NiCo_2O_4$, respectively. The obtained XRD pattern closely matched the JCPDS No. 20-0781 standard card [37], confirming the successful synthesis of pure $NiCo_2O_4$ powders through the sono-hydrothermal method in which the absence of impurity peaks indicates that the $NiCo_2O_4$ is free from significant contamination from other phases.

SEM analysis highlights the structure, particle size, and distribution of the synthesized nanomaterials and to this extent, an SEM image of the $NiCo_2O_4$ catalyst is

shown in Figure 2b. The structure of the electrocatalyst is flower-like nanorods, homogeneous in a single-shaped structure. The reason behind this well-established morphology not only corresponds to the good nucleation caused by sonication but also to the existence of the hydrolysis agent, urea, which bonds Ni^{2+} and Co^{2+} ions together.

To confirm the results obtained through XRD and SEM, EDS analysis was performed, and this characterization is shown in Figure 2c. Three different areas of electrocatalyst were selected, and EDS was performed to unravel the distribution of the elements in the structure of Ni–Co metal. Based on the results, only Ni, Co, and O elements are present in the structure; the weight percentages follow the theoretical molar ratio of the $NiCo_2O_4$, ensuring that the synthesis methods were appropriate throughout the sono-hydrothermal route.

TEM analysis was performed and results are shown in Figure 2d, in order to gain better insight into the $NiCo_2O_4$ electrocatalyst. The dimensions of the particles are between 20 and 45 nm, further confirming the advantage of the sono-hydrothermal method in the formation of homogeneous nanoparticles. Also, a lattice spacing of 0.246 nm was observed, which is related to the (311) plane of $NiCo_2O_4$ electrocatalyst.

Based on the results of XRD, SEM, EDS, and TEM, the synthesized electrocatalyst is Ni–Co metal oxide, mainly $NiCo_2O_4$ spinel type catalyst in a pure form, with flower-shaped structures made of homogeneous nano-needles. Sonication for the synthesis process promotes widespread particle distribution by increasing the nucleation rate. It results in a larger number of uniform small nuclei, which leads to reduced aggregation and formation of smaller particles [38]. Also, urea as a hydrolysis agent can help bond ions of Ni and Co more easily, achieving a pure and single-phase morphology $NiCo_2O_4$ electrocatalyst.

3.2. Electrochemical Characterization

The results of the electrochemical tests carried out on the hybrid $NiCo_2O_4$@NiFelt electrode using different REs and at different temperatures and pH are reported here. More details on the performance of the catalyst and its comparison with results from the literature on $NiCo_2O_4$ can be found in [10].

3.2.1. Changing the Reference Electrode

Figure 3 illustrates the OER properties of synthesized Ni–Co metal oxide on NiFelt and clean bare NiFelt, obtained with two different REs. Hybrid $NiCo_2O_4$@NiFelt electrodes were tested as anodes to evaluate their electrocatalytic performance for the OER in a 1.0 M KOH solution at T = 20 °C. Platinum foil was used as the counter electrode while Hg/HgO or Ag/AgCl were utilized as the RE.

This OER reaction involves multiple proton-coupled electron transfer steps, requiring efficient catalysts to lower the overpotential and enhance the reaction rate. Since the electrolyte is KOH, there are OH^- ions in the solution. Firstly, the hybrid $NiCo_2O_4$ on the NiFelt electrode surface adsorbs hydroxide ions from the electrolyte. These ions undergo a transformation, forming intermediate species on the electrode surface. In the second step, these intermediate species interact to form bonds between oxygen atoms. The oxygen molecules formed on the surface of the $NiCo_2O_4$ on the NiFelt electrode are then released into the electrolyte. The entire process theoretically requires four electrons.

The working electrode tested by the Hg/HgO RE is named NiCo-Hg, while the same electrode tested with the Ag/AgCl RE is named NiCo-Ag. Bare NiFelt was tested just by the Hg/HgO RE, and it is named NiFelt-Hg. In Figure 3a, linear sweep voltammetry (LSV) results are reported, performed at a scan rate of 5 mV/s. The results are corrected for 100% iR drop. By looking at the LSV outcomes, the electrochemical activity of hybrid $NiCo_2O_4$@NiFelt anode is significantly improved in comparison to bare NiFelt: at 50 mA/cm^2, the overpotentials for NiCo-Ag, NiCo-Hg, and NiFelt-Hg are 310, 350, and 435.3 mV, respectively, highlighting the good performance of the synthesized electrode and showing that the overpotential obtained by Ag/AgCl is lower than that measured by

Hg/HgO. Another significant difference is related to the anodic peak for NiCo-Hg, which is higher in comparison to that obtained by NiCo-Ag. This difference can be associated with the theoretical formula used for the conversion to RHE and to the different sensitivity of the RE for the basic solution, which is supposed to be amplified at high current densities.

Figure 3b compares overpotentials for NiCo-Hg, NiCo-Ag, and NiFelt-Hg at 10 mA/cm^2 and 50 mA/cm^2, obtained by backward LSV. At a standard current density (10 mA/cm^2), the overpotentials for NiCo-Ag, NiCo-Hg, and NiFelt-Hg are 278, 288, and 396.9 mV, respectively. At this lower current density, the difference between the overpotential measured for Ag/AgCl and Hg/HgO is 10 mV, less than the previously calculated one, as expected.

Electrochemical impedance spectroscopy (EIS) was carried out for the NiCo-Hg, NiCo-Ag, and NiFelt-Hg electrodes at the open circuit voltage (OCV) to examine the system's transport properties, and the results are reported in Figure 3c. An equivalent circuit was derived through data analysis to evaluate the results. The uncompensated solution resistance (R_S), which was totally iR corrected for the LSV curves, was calculated with both Ag/AgCl and Hg/HgO. The values were determined to be 1.18 and 1.22 Ω, respectively. The diameter of the semicircle can reveal the charge transfer resistance for the electrode under evaluation. The first realized result shows that the hybrid $NiCo_2O_4$@NiFelt electrode exhibits excellent resistance reduction in comparison to bare NiFelt. This confirms that the catalyst morphology observed by SEM and TEM, i.e., the nanorods-flower-like shape, can facilitate mass transfer. The charge transfer resistance (R_{ct}) values for NiCo-Hg, NiCo-Ag, and NiFelt-Hg are 2.1, 1.98, and 3.78 Ω, respectively. The results obtained by the Ag/AgCl reference electrode in comparison to Hg/HgO show lower measured resistance at about 6% difference, which can be not only related to the sensitivity of the RE but also to the solution inside the RE, being 3M KCl for Ag/AgCl and 1M KOH for Hg/HgO.

The Tafel slope was calculated by backward LSV as an activity indicator of the hybrid $NiCo_2O_4$@NiFelt electrode, and results are reported in Figure 3d. For NiCo-Hg and NiCo-Ag, the calculated slopes are 89 and 90 mV/dec, respectively. This is just about a 1% difference, which is statistically not significant.

To understand the activity of the $NiCo_2O_4$ hybridized with NiFelt, electrochemical active surface area (ECSA) was calculated for both NiCo-Hg and NiFelt-Hg in 1 M KOH, 20 °C temperature, using CV with different scan rates, and the results are shown in Figures S1 and S2. Also, the capacitance double layer values for NiCo-Hg and NiFelt-Hg, which are depicted in Figure S3, are 2.55 and 0.886 mF/cm^2, respectively. For the ECSA values, NiCo-Hg showed 63.75 cm^2, and this was 22.5 cm^2 for NiFelt-Hg, which show significant increases in the ECSAs and respective OER performances using a binder-free method.

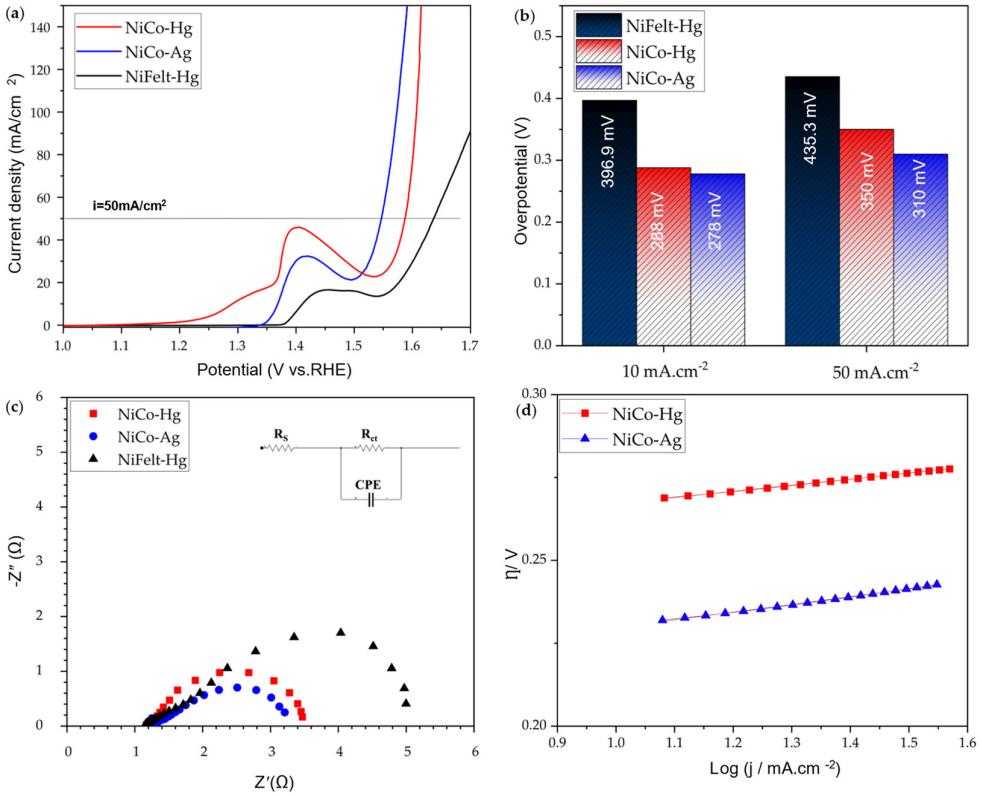

Figure 3. OER tests of NiCo-Hg, NiCo-Ag, and NiFelt-Hg: (**a**) 100% iR-corrected LSV, (**b**) overpotentials, (**c**) EIS, (**d**) Tafel plot.

From the previous results, it is understood that the choice in measuring the polarization curve and resistance through EIS with Ag/AgCl and Hg/HgO poses some differences but not in a way that alters so much the results obtained.

The CV test is another important electrochemical activity test that can show the redox properties of the electrodes. Moreover, multistep chronopotentiometry and multistep chronoamperometry can provide information about the short stability of the tested electrode. Also, these tests were performed using different Res, and the results are reported in Figure 4.

Figure 4a,b show the CVs for the hybrid $NiCo_2O_4$@NiFelt electrode measured with Hg/HgO RE and Ag/AgCl RE, respectively. Five different scan rates ranging from 10 mV/s to 50 mV/s with a 10 mV step rate were studied to show the redox reaction of Ni to Ni^{2+} and Co to Co^{2+}. Initially, the CV curve obtained with Ag/AgCl is more symmetric and well shows the anodic and cathodic peaks. In particular, at a 10 mV/s scan rate, the anodic peak is about 1.52 V vs. RHE using Hg/HgO RE (Figure 4a), while it is 1.46 V vs. RHE with Ag/AgCl RE (Figure 4b).

This difference in shift can arise from the theoretical formula used for the calibration of the RE, which means the best way would be to calibrate the reference electrode with the saturated calomel electrode (SCE) to minimize the error as much as possible. It can be noticed that this shift is constant both for anodic and cathodic peaks when comparing results obtained with Ag/AgCl and Hg/HgO. The significant outcome would be related to the symmetric curve (reduction and oxidation) of the CV calculated for Ag/AgCl. It seems that Ag/AgCl can show a higher current density, making it the better option for capacitance calculation and studying supercapacitors and battery applications, even if it is not a good electrode in basic solution.

To go further, multistep chronopotentiometry (Figure 4c) and multistep chronoamperometry (Figure 4d) were performed with both Ag/AgCl and Hg/HgO with 6

different steps for 100 s per step. By considering Figure 4c, multistep chronopotentiometry was carried out by increasing the current density from 10 mA/cm² to 60 mA/cm² with a 10 mA/cm² increase in each step. The hybrid $NiCo_2O_4$@NiFelt electrode was stable during the measurement with both reference electrodes, although NiCo-Hg showed a 30 mV higher potential than NiCo-Ag. Looking at Figure 4c, it can be noticed that the response curve at increasing current using Ag/AgCl as RE is slower than that using Hg/HgO; moreover, this different behavior was not observed with chronoamperometry.

Figure 4d shows the multistep chronoamperometry carried out in 6 steps starting from 350 mV up to 600 mV with a 50 mV increment at each step. As can be seen, the results are in accordance with the multistep chronopotentiometry; for instance, at 350 mV, NiCo-Hg achieves 98 mA while NiCo-Ag achieves 112 mA.

In summary, Ag/AgCl is a good choice for capacitance measurement and also for detecting the anodic and cathodic peaks, as the area under the CV curve is more symmetric. As a result, choosing between Ag/AgCl and Hg/HgO is an important factor, as it seems that Ag/AgCl in basic solution can overestimate the performance and show lower overpotential in higher current densities; however, at lower current densities and lower scan rates, the results obtained for Ag/AgCl and Hg/HgO are similar with only a slight difference.

Our results are in agreement with [39], in which different types of electrodes in alkaline, acidic, and neutral waters were analyzed to assess how the pH can shift the potential, and with [40], in which Hg/HgO RE was studied at different concentrations of NaOH/KOH electrolyte.

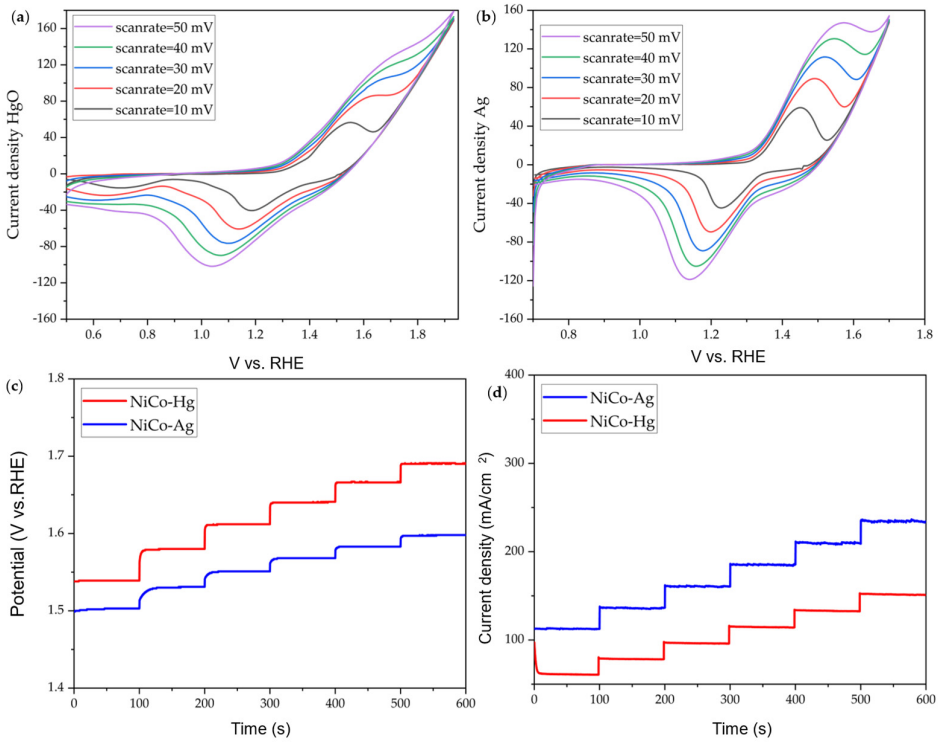

Figure 4. OER tests of NiCo-Hg and NiCo-Ag: (**a**) CV of NiCo-Hg, (**b**) CV of NiCo-Ag, (**c**) multistep chronopotentiometry, (**d**) multistep chronoamperometry.

3.2.2. Changing Electrolyte pH and Operating Temperature

The OER performance of the hybrid $NiCo_2O_4$@NiFelt electrode was further evaluated at different KOH concentrations (0.25, 0.5, and 1.0 M) and different temperatures starting from 20 °C up to 80 °C, and results are reported in Figure 5. In these experiments, the reference electrode Ag/AgCl was used as it seems more sensitive compared to Hg/HgO, and because at higher temperatures Hg can dissolve inside the solution.

Figure 5a shows 100% iR-corrected backward LSV data with a 5 mv/s scan rate for the hybrid $NiCo_2O_4$@NiFelt electrode in different KOH concentrations. At 10 mA/cm^2, the overpotentials for 1 M, 0.5 M, and 0.25 M KOH are 278, 287, and 300 mV, respectively. There is a slight difference between these results that is related to the conductivity of the electrolyte with higher-molarity KOH. Thus, the higher molarity improves the electrochemical activity, as expected.

Figure 5b illustrates the EIS in different KOH molarities. The solution resistances for 0.5 M and 1.0 M are roughly at the same level at about 1.18 and 1.28 Ω, respectively, which highlights the fact that there are enough ions inside the electrolyte to facilitate the charge transfer. In terms of charge transfer resistance, the values calculated for 1.0 M KOH and 0.5 M KOH are 1.98 and 2.0 Ω, respectively, suggesting the 0.5 M KOH can be a good choice for three-electrode test measurement as the results are just 1% different at a 50% lower concentration. On the other side, for 0.25 M KOH, a lot of noise was observed and the analysis was performed two other times, but the only obvious thing is that the electrolyte resistance is much higher at about 4.4 Ω. A good way to consider the electrochemical activity in a lower concentration of electrolytes for this catalyst would be to use a rotating disk electrode to reduce the noise during EIS, but all in all, KOH = 0.5 M seems to be the appropriate concentration even for using Ag/AgCl as a reference electrode in a conventional three-electrode setup.

A further step was taken to study the performance of the hybrid $NiCo_2O_4$@NiFelt electrode at different temperatures (20, 40, 60, and 80 °C) using Ag/AgCl as RE. The potential reported is related to Ag/AgCl without iR correction; the results are reported in Figure 5c for backward LSV and Figure 5d for EIS in 1.0 M KOH.

If we look at Figure 5c, at a current density of 10 mA/cm^2, at 20, 40, 60, and 80 °C, the potentials vs. Ag/AgCl are 510, 490, 430, and 410 mV, respectively. It is obvious that by increasing the temperature from 20 °C to 80 °C, the potential is decreased by 100 mV (20%), which means temperature can increase the overall electrochemical activity of the electrocatalyst. Also, by looking at the cathodic peak, it can be realized that the higher the temperature, the bigger the curve. It is meaningful that the numbers of redox species such as Ni^{2+} and Co^{2+} are higher on the surface of the electrocatalyst, facilitating ion and electrical charge transfer.

Figure 5d shows the EIS and resistance taken at different temperatures. The solution resistance is the same for all the temperatures at about 1.22 Ω. For charge transfer resistances, at 20, 40, 60, and 80 °C, the R_{ct} values are 1.98, 1.88, 1.86, and 1.5, respectively, which agree with the results already obtained from backward LSV at different temperatures.

The results of Figure 5 are in agreement with [41]; the influence of the temperature on Co-based catalysts for oxygen evolution reactions was deeply studied in an alkaline environment.

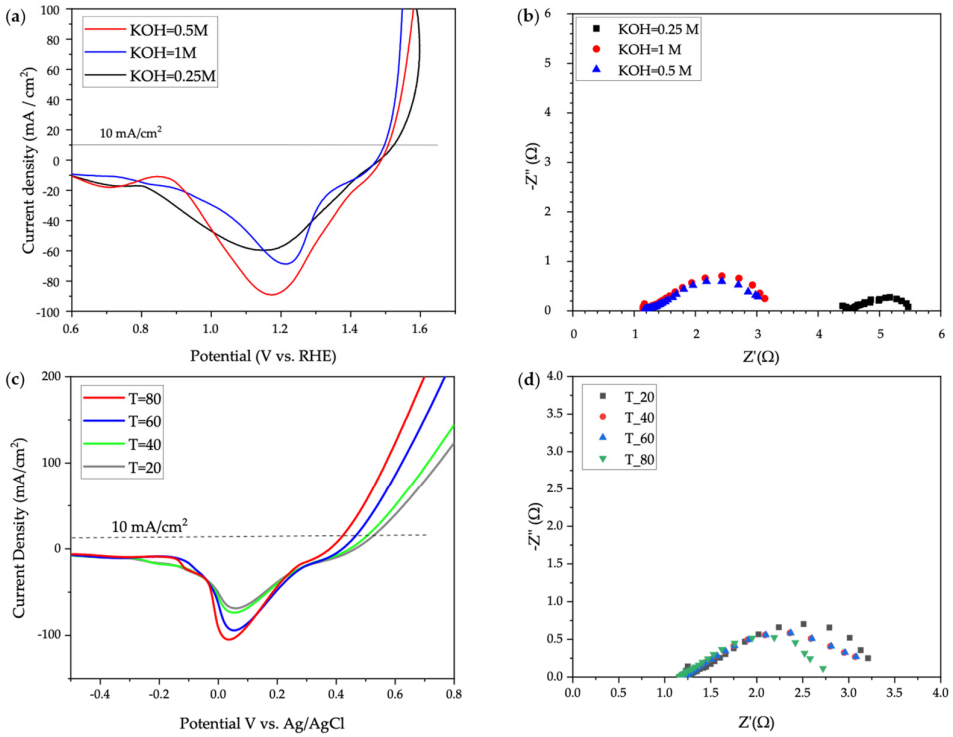

Figure 5. OER studies of NiCo-Ag for different KOH concentrations and temperatures: (**a**) LSV data for NiCo-Ag in different KOH molarities, (**b**) EIS data for NiCo-Ag in different KOH molarities, (**c**) LSV data for NiCo-Ag at different temperatures, (**d**) EIS data for NiCo-Ag at different temperatures.

3.3. Stability Tests

To evaluate the stability and long-term usability of hybrid $NiCo_2O_4$@NiFelt electrodes, CVs as electrochemical analysis in combination with physicochemical analysis were performed. Results are reported in Figure 6.

A thousand cycles of CV with a 50 mV/s scan rate were carried out in 1 M KOH using Ag/AgCl as RE and Pt wire as a counter electrode. As can be seen in Figure 6a, the electrode polarization curve is constant after 1000 CVs, and at 10 mA/cm² the overpotential is changed by about 2 mV. Even EIS values before and after stability (Figure 6b) show the same behavior, the resistance increased from 1.98 to 2.13 Ω.

The cathodic peak after 1000 CV cycles is much higher, which can be related to the change in morphology from spinel structure ($NiCo_2O_4$) to Ni^{2+} and Co^{2+} and remaining in this state. To understand this phenomenon, physicochemical analysis was performed starting from XRD analysis, for which results are reported in Figure 6c. By comparing the XRD peaks at 18.90°, 31.15°, 36.70°, 38.40°, 44.62°, 55.43°, 59.09°, 64.98°, and 77.54°, no difference was observed in terms of shifts of peaks, and the electrocatalyst is in accordance with JCPDS No. 20-0781 standard even after 1000 CV cycles. The intensity of peaks reduced a little bit, which can be related to the small number of metal ions existing on the surface of the electrocatalyst. Consequently, SEM and EDS were performed to confirm this hypothesis. Figure 6d shows SEM imagery of Ni–Co oxide powder, which was scratched from the NiFelt electrode after the stability test. The morphology remained stable as it was in the fresh state, clearly showing nanorod-flower morphology. Also, EDS analysis was performed for the powder (Figure 6e), and the elements are consistent with the theoretical values.

After these analyses, it is possible to conclude that metal particles on the $NiCo_2O_4$ are converted to Ni and Co ions on the surface and facilitate charge transfer easily, but in

spinel form and not in metal form, and leach from the surface. This was already confirmed by XRD, SEM, and EDS analyses after the stability test.

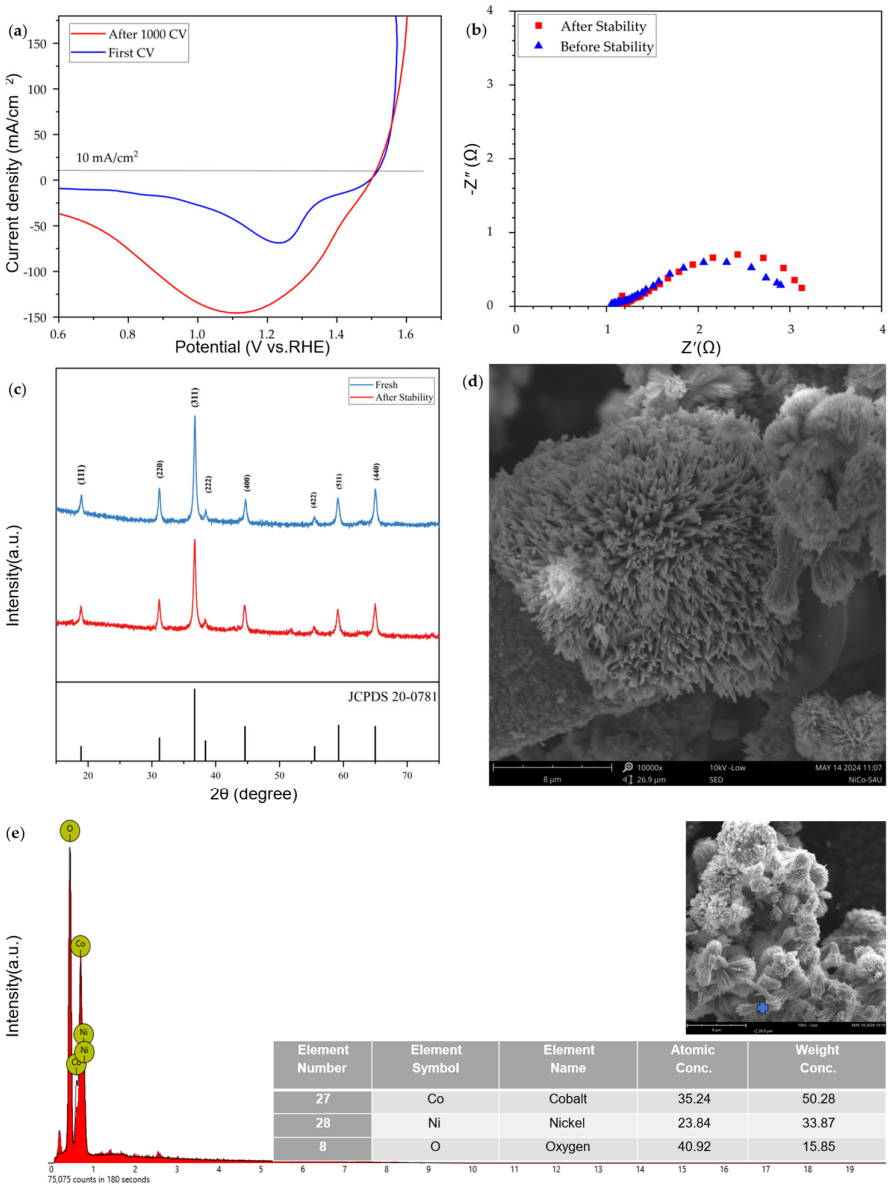

Element Number	Element Symbol	Element Name	Atomic Conc.	Weight Conc.
27	Co	Cobalt	35.24	50.28
28	Ni	Nickel	23.84	33.87
8	O	Oxygen	40.92	15.85

Figure 6. Stability and long-term usability of hybrid $NiCo_2O_4$@NiFelt electrode: (**a**) Backward LSV before and after stability, (**b**) EIS data before and after stability, (**c**) XRD analysis before and after stability, (**d**) SEM analysis after stability, (**e**) EDS results after stability.

4. Conclusions

In this study, a hybrid $NiCo_2O_4$@NiFelt electrode was produced by a sono-hydrothermal method to be used for OERs in alkaline environments. Physical–chemical analysis confirmed that pure $NiCo_2O_4$, with homogeneous nanorod structure and particle dimensions between 20 and 45 nm, is hybridized on the electrode surface.

The electrochemical performances of the hybrid $NiCo_2O_4$@NiFelt electrode were assessed at different KOH concentrations and temperatures using Ag/AgCl as a reference electrode. Higher KOH molarity and temperatures improved the catalyst's electrochemical activity, as expected.

Electrochemical tests were also conducted using an Hg/HgO reference electrode for comparing results. Using Ag/AgCl generally showed lower overpotentials and higher current densities, making Ag/AgCl a good choice, at a lower price, for capacitance measurements and redox peak detection in cyclic voltammetry at not strong alkaline pH, like that in AEM water electrolysis.

Stability tests carried out with 1000 cycles of CV protocol highlighted good stability of the hybrid $NiCo_2O_4$@NiFelt electrode: only minor changes in resistance and overpotential were observed, indicating good long-term stability. Further physical–chemical analyses were carried out to verify the catalyst structure and composition after electrode use, showing that the electrocatalyst did not degrade by maintaining the same structure and composition.

Overall, the tests highlighted the good performance and stability of the proposed electrode made of low-cost transition metal oxide on Ni felt, suggesting its use at an industrial scale. Moreover, our results underlined how it is important to pay attention to the choice of the correct reference electrode, which can significantly impact the measurement outcomes.

Supplementary Materials: The following supporting information can be downloaded at: https://www.mdpi.com/article/10.3390/en17153703/s1, Figure S1: CV of $NiCo_2O_4$ with Hg/HgO reference electrode with a different scan rate; Figure S2; CV of NiFelt with Hg/HgO reference electrode with a different scan rate; Figure S3: Capacitance double layer calculation $NiCo_2O_4$@NiFelt and bare NiFelt.

Author Contributions: A.N.: conceptualization, methodology, investigation, formal analysis, visualization, writing—original draft, writing—review and editing. A.M.: conceptualization, validation, writing—original draft, writing—review and editing. P.B.A.: analysis, investigation. F.M.N.: analysis, investigation. O.P.: ! conceptualization, writing—reviewing and editing, supervision, project administration, funding acquisition. All authors have read and agreed to the published version of the manuscript.

Funding: The present study was funded by the EU Next Generation—PNRR, M2C213.5, project NEMESI_ID: RSH2B_000002, CUP: F39J22001960004, and by the PhD grant FSE + 2021–2027, ESO 4.6 at the University of Genova, Italy.

Data Availability Statement: The original contributions presented in the study are included in the article/supplementary material; further inquiries can be directed to the corresponding author/s.

Acknowledgments: The authors wish to thank Antonio Comite (Head of Elemental lab at DCCI, Department of Chemistry of the University of Genoa) and Laura Negretti, who carried out TEM analyses at DCCI. Thanks to Alessio Costa from Ansaldo Energia S.p.A. for conducting SEM and EDS analyses. Thanks to Juan Felipe Basbus from DICCA, University of Genoa, for carrying out XRD analysis.

Conflicts of Interest: The authors declare no conflicts of interest.

References

1. Zong, N.; Wang, J.; Liu, Z.; Wu, S.; Tong, X.; Kong, Q.; Xu, R.; Yang, L. Electrode Materials with High Performance of Nickel Sulfide/Titanium Nitride@Co-Based Metal–Organic Frameworks/Nickel Foam for Supercapacitors. *Energies* **2024**, *17*, 2788. https://doi:10.3390/en17112788.
2. Jeong, J.-Y.; Lee, J.M.; Park, Y.S.; Jin, S.; Myeong, S.-W.; Heo, S.; Lee, H.; Albers, J.G.; Choi, Y.-W.; Seo, M.H.; et al. High-Performance RuO2/CNT Paper Electrode as Cathode for Anion Exchange Membrane Water Electrolysis. *Appl. Catal. B Environ. Energy* **2024**, *356*, 124220. https:// doi:10.1016/j.apcatb.2024.124220.
3. Criteria Air Pollutants and Greenhouse Gas Emissions from Hydrogen Production in U.S. Steam Methane Reforming Facilities | Environmental Science & Technology Available online: https://pubs.acs.org/doi/10.1021/acs.est.8b06197 (accessed on 10 June 2024).
4. Xu, Q.; Zhang, L.; Zhang, J.; Wang, J.; Hu, Y.; Jiang, H.; Li, C. Anion Exchange Membrane Water Electrolyzer: Electrode Design, Lab-Scaled Testing System and Performance Evaluation. *EnergyChem* **2022**, *4*, 100087. https://doi:10.1016/J.ENCHEM.2022.100087.

5. Linden, F.V.D.; Pahon, E.; Morando, S.; Bouquain, D. A Review on the Proton-Exchange Membrane Fuel Cell Break-in Physical Principles, Activation Procedures, and Characterization Methods. *J. Power Sources* **2023**, *575*, 233168. https://doi:10.1016/j.jpowsour.2023.233168.
6. Huang, S.; Yuan, Z.; Salla, M.; Wang, X.; Zhang, H.; Huang, S.; Lek, D.G.; Li, X.; Wang, Q. A Redox-Mediated Zinc Electrode for Ultra-Robust Deep-Cycle Redox Flow Batteries. *Energy Environ. Sci.* **2023**, *16*, 438–445. https:// doi:10.1039/D2EE02402K.
7. Yang, G.; Zhu, Y.; Hao, Z.; Lu, Y.; Zhao, Q.; Zhang, K.; Chen, J. Organic Electroactive Materials for Aqueous Redox Flow Batteries. *Adv. Mater.* **2023,** *35*, 230189 https://, doi:10.1002/adma.202301898.
8. Bonizzoni, S.; Stucchi, D.; Caielli, T.; Sediva, E.; Mauri, M.; Mustarelli, P. Morpholinium-Modified, Polyketone-Based Anion Exchange Membranes for Water Electrolysis. *ChemElectroChem* **2023**, *10*, e202201077. https://doi:10.1002/celc.202201077.
9. Chand, K.; Paladino, O. Recent Developments of Membranes and Electrocatalysts for the Hydrogen Production by Anion Exchange Membrane Water Electrolysers: A Review. *Arab. J. Chem.* **2023**, *16*, 104451. https://doi:10.1016/j.arabjc.2022.104451.
10. Niyati, A.; Moranda, A.; Basbus, J.F.; Paladino, O. Unlocking the Potential of NiCo2O4 Nanocomposites: Morphology Modification Based on Urea Concentration and Hydrothermal and Calcination Temperature. *New J. Chem.* **2024**, *48*, 11035–11043. https://doi:10.1039/D4NJ01581A.
11. Niyati, A.; Moranda, A.; Navarra, F.; Riva, A.; Campione, M.; Schiappelli, G.; Paladino, O. Design of the Experiments for the Selection of Potential Electrocatalysts for Both AEM Electrolyzers and Redox Flow Batteries. *E3S Web Conf.* **2023**, *414*, 01002. https://doi:10.1051/e3sconf/202341401002.
12. Wan, L.; Liu, J.; Lin, D.; Xu, Z.; Zhen, Y.; Pang, M.; Xu, Q.; Wang, B. 3D-Ordered Catalytic Nanoarrays Interlocked on Anion Exchange Membranes for Water Electrolysis. *Energy Environ. Sci.* **2024**, *17*, 3396–3408. https:// doi:10.1039/D4EE00003J.
13. Yang, L.; Shui, J.; Du, L.; Shao, Y.; Liu, J.; Dai, L.; Hu, Z. Carbon-Based Metal-Free ORR Electrocatalysts for Fuel Cells: Past, Present, and Future. *Adv. Mater.* **2019**, *31*, 1804799. https://doi:10.1002/adma.201804799.
14. Liu, C.; Lin, B.; Zhang, H.; Wang, Y.; Wang, H.; Tang, J.; Zou, C. Influence of Power Fluctuation on Ni-Based Electrode Degradation and Hydrogen Evolution Reaction Performance in Alkaline Water Splitting: Probing the Effect of Renewable Energy on Water Electrolysis. *Catalysts* **2024**, *14*, 307. https://doi:10.3390/catal14050307.
15. Guo, B.; Ding, Y.; Huo, H.; Wen, X.; Ren, X.; Xu, P.; Li, S. Recent Advances of Transition Metal Basic Salts for Electrocatalytic Oxygen Evolution Reaction and Overall Water Electrolysis. *Nano-Micro Lett.* **2023**, *15*, 57. https://doi:10.1007/s40820-023-01038-0.
16. Moysiadou, A.; Hu, X. Stability Profiles of Transition Metal Oxides in the Oxygen Evolution Reaction in Alkaline Medium. *J. Mater. Chem. A* **2019**, *7*, 25865–25877. https://doi:10.1039/C9TA10308B.
17. Song, F.; Bai, L.; Moysiadou, A.; Lee, S.; Hu, C.; Liardet, L.; Hu, X. Transition Metal Oxides as Electrocatalysts for the Oxygen Evolution Reaction in Alkaline Solutions: An Application-Inspired Renaissance. *J. Am. Chem. Soc.* **2018**, *140*, 7748–7759. https:// doi:10.1021/jacs.8b04546.
18. Osgood, H.; Devaguptapu, S.V.; Xu, H.; Cho, J.; Wu, G. Transition Metal (Fe, Co, Ni, and Mn) Oxides for Oxygen Reduction and Evolution Bifunctional Catalysts in Alkaline Media. *Nano Today* **2016**, *11*, 601–625. https://doi:10.1016/j.nantod.2016.09.001.
19. Flores-Lasluisa, J.X.; Huerta, F.; Cazorla-Amorós, D.; Morallón, E. Transition Metal Oxides with Perovskite and Spinel Structures for Electrochemical Energy Production Applications. *Environ. Res.* **2022**, *214*, 113731. https:// doi:10.1016/j.envres.2022.113731.
20. Liu, X.-M.; Cui, X.; Dastafkan, K.; Wang, H.-F.; Tang, C.; Zhao, C.; Chen, A.; He, C.; Han, M.; Zhang, Q. Recent Advances in Spinel-Type Electrocatalysts for Bifunctional Oxygen Reduction and Oxygen Evolution Reactions. *J. Energy Chem.* **2021**, *53*, 290–302. https://doi:10.1016/j.jechem.2020.04.012.
21. Zhao, Q.; Yan, Z.; Chen, C.; Chen, J. Spinels: Controlled Preparation, Oxygen Reduction/Evolution Reaction Application, and Beyond. *Chem. Rev.* **2017**, *117*, 10121–10211. https://doi:10.1021/acs.chemrev.7b00051.
22. Liu, S.; Hu, L.; Xu, X.; Al-Ghamdi, A.A.; Fang, X. Nickel Cobaltite Nanostructures for Photoelectric and Catalytic Applications. *Small* **2015**, *11*, 4267–4283. https://doi:10.1002/smll.201500315.
23. Hu, L.; Wu, L.; Liao, M.; Hu, X.; Fang, X. Electrical Transport Properties of Large, Individual NiCo2O4 Nanoplates. *Adv. Funct. Mater.* **2012**, *22*, 998–1004. https://doi:10.1002/adfm.201102155.
24. Sudarsono, W.; Tan, S.Y.; Wong, W.Y.; Omar, F.S.; Ramya, K.; Mehmood, S.; Numan, A.; Walvekar, R.; Khalid, M. From Catalyst Structure Design to Electrode Fabrication of Platinum-Free Electrocatalysts in Proton Exchange Membrane Fuel Cells: A Review. *J. Ind. Eng. Chem.* **2023**, *122*, 1–26. https://doi:10.1016/j.jiec.2023.03.004.
25. Chatterjee, M.; Saha, S.; Das, S.; Pradhan, S.K. Advanced Asymmetric Supercapacitor with NiCo2O4 Nanoparticles and Nanowires Electrodes: A Comparative Morphological Hierarchy. *J. Alloys Compd.* **2020**, *821*, 153503. https:// doi:10.1016/J.JALLCOM.2019.153503.
26. Yadav, S.; Sharma Ghrera, A.; Devi, A. Hierarchical Grass-like NiCo2O4 Nanowires Grown on Nickel Foam as a Binder-Free Supercapacitor Electrode. *Mater. Today Proc.* **2023**, *74*, 281–288. https://doi:10.1016/J.MATPR.2022.08.240.
27. Packiaraj, R.; Devendran, P.; Venkatesh, K.S.; Mahendraprabhu, K.; Nallamuthu, N. Unveiling the Structural, Charge Density Distribution and Supercapacitor Performance of NiCo2O4 Nano Flowers for Asymmetric Device Fabrication. *J. Energy Storage* **2021**, *34*, 102029. https://doi:10.1016/j.est.2020.102029.
28. Zhang, X.; Yang, F.; Chen, H.; Wang, K.; Chen, J.; Wang, Y.; Song, S. In Situ Growth of 2D Ultrathin $NiCo_2O_4$ Nanosheet Arrays on Ni Foam for High Performance and Flexible Solid-State Supercapacitors. *Small* **2020**, *16*, e2004188. https://doi:10.1002/smll.202004188.

29. Yang, G.; Park, S.J. Facile Hydrothermal Synthesis of NiCo2O4- Decorated Filter Carbon as Electrodes for High Performance Asymmetric Supercapacitors. *Electrochimica Acta* **2018**, *285*, 405–414. https://doi:10.1016/J.ELECTACTA.2018.08.013.
30. Liu, Z.Q.; Xu, Q.Z.; Wang, J.Y.; Li, N.; Guo, S.H.; Su, Y.Z.; Wang, H.J.; Zhang, J.H.; Chen, S. Facile Hydrothermal Synthesis of Urchin-like NiCo2O4 Spheres as Efficient Electrocatalysts for Oxygen Reduction Reaction. *Int. J. Hydrog. Energy* **2013**, *38*, 6657–6662. https://doi:10.1016/J.IJHYDENE.2013.03.092.
31. Wu, Z.; Pu, X.; Zhu, Y.; Jing, M.; Chen, Q.; Jia, X.; Ji, X. Uniform Porous Spinel NiCo2O4 with Enhanced Electrochemical Performances. *J. Alloys Compd.* **2015**, *632*, 208–217. https://doi:10.1016/J.JALLCOM.2015.01.147.
32. Yadav, D.; Singh, P.; Prasad, R. Advanced Thermally Stable, Self-Sustaining NiCo2O4 Catalyst for CNG Emissions in Lean Burn Environment. *Int. J. Hydrog. Energy* **2019**, *44*, 29057–29065. https://doi:10.1016/J.IJHYDENE.2019.08.238.
33. Kaur, M.; Chand, P.; Anand, H. Binder Free Electrodeposition Fabrication of NiCo2O4 Electrode with Improved Electrochemical Behavior for Supercapacitor Application. *J. Energy Storage* **2022**, *52*, 104941. https://doi:10.1016/J.EST.2022.104941.
34. Shchegolkov, A.V.; Lipkin, M.S.; Shchegolkov, A.V.; Korbova, E.V.; Lipkina, T.V.; Lipkin, V.M. On the Mechanism of Formation of Electrochromic WO3 Films on the Surface of Sn, Ti, ITO Electrodes in the Process of Cathodic Electrodeposition. *Inorg. Mater. Appl. Res.* **2022**, *13*, 1605–1614. https://doi:10.1134/S2075113322060223.
35. Kaur, M.; Chand, P.; Anand, H. Facile Synthesis of NiCo2O4 Nanostructure with Enhanced Electrochemical Performance for Supercapacitor Application. *Chem. Phys. Lett.* **2022**, *786*, 139181. https://doi:10.1016/J.CPLETT.2021.139181.
36. Yan, S. xue; Luo, S. hua; Sun, M. zhu; Wang, Q.; Zhang, Y. hui; Liu, X. Facile Hydrothermal Synthesis of Urchin-like NiCo2O4 as Advanced Electrochemical Pseudocapacitor Materials. *Int. J. Energy Res.* **2021**, *45*, 20186–20198. https://doi:10.1002/ER.7101.
37. Lei, Y.; Li, J.; Wang, Y.; Gu, L.; Chang, Y.; Yuan, H.; Xiao, D. Rapid Microwave-Assisted Green Synthesis of 3D Hierarchical Flower-Shaped NiCo2O4 Microsphere for High-Performance Supercapacitor. *ACS Appl. Mater. Interfaces* **2014**, *6*, 1773–1780. https:// doi:10.1021/am404765y.
38. Niyati, A.; Haghighi, M.; Shabani, M. Solar-Assisted Photocatalytic Elimination of Azo Dye Effluent Using Plasmonic AgCl Anchored Flower-like Bi4O5I2 as Staggered Nano-Sized Photocatalyst Designed via Sono-Precipitation Method. *J. Taiwan Inst. Chem. Eng.* **2020**, *115*, 144–159. https://doi:10.1016/j.jtice.2020.10.012.
39. Anantharaj, S.; Sagayaraj, P.J.J.; Yesupatham, M.S.; Arulraj, R.; Eswaran, K.; Sekar, K.; Noda, S. The Reference Electrode Dilemma in Energy Conversion Electrocatalysis: "Right vs. Okay vs. Wrong." *J. Mater. Chem. A* **2023**, *11*, 17699–17709. https:// doi:10.1039/d3ta03145d.
40. Kawashima, K.; Márquez, R.A.; Son, Y.J.; Guo, C.; Vaidyula, R.R.; Smith, L.A.; Chukwuneke, C.E.; Mullins, C.B. Accurate Potentials of Hg/HgO Electrodes: Practical Parameters for Reporting Alkaline Water Electrolysis Overpotentials. *ACS Catal.* **2023**, *13*, 1893–1898. https://doi:10.1021/acscatal.2c05655.
41. Zhang, G.; Wang, H.; Yang, J.; Zhao, Q.; Yang, L.; Tang, H.; Liu, C.; Chen, H.; Lin, Y.; Pan, F. Temperature Effect on Co-Based Catalysts in Oxygen Evolution Reaction. *Inorg. Chem.* **2018**, *57*, 2766–2772. https://doi:10.1021/acs.inorgchem.7b03168.